Materials Science and Engineering B 119 (2005) 65–70

www.elsevier.com/locate/mseb

Effect of milling conditions on structure and magnetic properties of nanocrystalline cobalt

N. Feneniche[a], S. Guessasma[a,*], N. Abdelbaki[b]

[a] *LERMPS, Université de Technologie de Belfort-Montbéliard (UTBM), Site de Sevenans, 90010 Belfort Cedex, France*
[b] *FEPM, Université M'Hamed Bougara de Boumerdès (UMBB), Algeria*

Received 9 April 2004; received in revised form 29 November 2004; accepted 11 January 2005

Abstract

Milling process conditions are related to magnetic properties of nanocrystalline Co material. Experiments are carried out varying plateau rotation and vial velocities. Coercivity, crystallite size and percentage of the cubic phase are analyzed using a statistical methodology based on artificial neural network. Predicted results show that the combination of low plateau rotation velocity and high vial velocity can enhance the cubic phase formation and consequently the coercivity.

Keywords: Nanocrystallline Co; Milling conditions; Magnetic properties; Artificial neural network

1. Introduction

Among the traditional routes for plastic deformation, ball milling has become a widespread technique for the processing of equilibrium and non-equilibrium powder materials [1]. Extensive research has been carried out during the last decades on the allotropic phase transformation of cobalt [2–4]. This metal undergoes a phase transition, from hcp to fcc, when it is heated to above the thermodynamic equilibrium temperature, T_t = 695 K. Moreover, pure fcc Co has been obtained at room temperature after a high-energy ball milling process and in particles of nanometric sizes [5–8]. Indeed, since the hcp and fcc are both close packed structures, stacking faults usually play a key role in all the models describing the transformation, either when it is thermally activated or induced by a cold-work process [2–4]. Stacking faults are also known to play a crucial role in the magnetic properties of Co-based hexagonal alloys used in longitudinal and perpendicular recording media and are usually considered to bring about a magnetic softening of this kind of materials [9].

In this study, coercivity Hc, crystallite size D and the hcp–fcc phase transformation (cubic phase ratio) are analyzed using a statistical methodology based on artificial neural network. The aim is to predict and quantify the relationships between these parameters and milling conditions over a large range of process variables, which are represented by few experimental sets. These include plateau rotation and vial velocities.

2. Experimental procedure

Nanocrystalline Co was produced by ball milling. Elemental powders, with an average particle size of 50 μm and a mean grain size of 200 Å were introduced into a cylindrical tempered steel container (vial) of capacity 50 ml. Each container was loaded with three quenched steel (type 100C6) balls (diameter 1.5 cm, mass 14 g). The containers were sealed with a Teflon O-ring and the milling conducted in stationary air without exchange with laboratory atmosphere. The milling was carried out using the so-called G5 specially designed planetary high-energy machine which allows the independent choice of the shock frequency and the shock energy [9,10].

* Corresponding author. Tel.: +333 84 58 3129; fax: +333 84 58 3286.
E-mail address: sofiane.guessasma@utbm.fr (S. Guessasma).

0921-5107/$ – see front matter © 2005 Elsevier B.V. All rights reserved.
doi:10.1016/j.mseb.2005.01.011

The effective conditions during the mechanical alloying were the rotation speed of the disc on which the containers are fixed (Ω) and the rotation speed of the containers (ω).

The milling time was chosen to avoid excessive contamination from the friction and the impacts between the balls and the walls of the vials but this milling time is long enough to obtain nanocrystalline cobalt.

The volume percent of the α(fcc) and the hexagonal close-packed ε(hcp) phases ratios are evaluated from the intensity ratios: $I_{fcc}/(I_{hcp}+I_{hcp})$ for fcc phase and $I_{hcp}/(I_{hcp}+I_{hcp})$ for hcp phase. Experimental details, microstructure characterization and magnetic measurements have been shown elsewhere [10].

3. Artificial neural network

An artificial neural network was built to relate input parameters plateau rotation and vial velocities to output parameters (crystallite size, percentage of the cubic phase and coercivity). Each of these parameters is indexed by a neuron (Fig. 1). Each parameter is introduced in the network structure as a formatted value according to [11]

$$I_i = \frac{x_i - x_{i\min}}{x_i - x_{i\min}} \quad i = 1, 2 \tag{1}$$

where I_i is the input formatted value of parameter i, $x_{\max}$ and $x_{\min}$ are the maximum and minimum values associated to parameter i. These are summarized in Table 1.

Input and output values for each neuron in structure are related as follows:

$$O_{ki} = \frac{1}{1+\mathrm{e}^{-I_{ki}}} \tag{2}$$

Table 1
The neural computation parameters

Parameter	Optimized values
Hidden layers	2
Learning rule	Quick propagation

Parameter	Optimized values	
	ω (rpm)	Ω (rpm)
Inputs ($I=2$)		
Minimum	45	135
Maximum	440	385

Parameter	Optimized values
First layer (N_1)	Varied
Second layer (N_2)	Varied

Parameter	Optimized values		
	D (μm)	C (%)	Hc (Oe)
Outputs ($O=3$)			
Minimum	0	0	0
Maximum	250	100	400

where k and i are the indexes of neuron k in the forward layer i.

Eq. (2) represents a nonlinear transformation of the input of each neuron in the structure assuming a sigmoid profile.

Neurons are related to each other with the aid of numbers translating the strength of the connection. These are called weights:

$$I_{ki} = w_{ijk} O_{kj} + w_{i0k} \tag{3}$$

k, i, j are subscripts designing the layer number, forward and backward layer, respectively, w_{i0k} represents a bias term. The summation is made on j values following Einstein notation.

Initially, weight parameters are not known and are tuned in order to decrease the difference between output layer values (y_i) and real case values corresponding to a submitted input case (I_i). Thus, calculation starts with

$$w_{ijk} = 1, \qquad E = \frac{1}{2}(r_i - y_i)^2, \quad i = 1, 3 \tag{4}$$

where E is the system energy which represents the quadratic variation of the error between real output values (r_i) and predicted values (y_i). The factor 1/2 is needed for derivation.

Weight update is performed by back-propagating the gradient of E from the output layer to the input layer. Weight correction is performed assuming the quick propagation algorithm [12]:

$$\Delta w_{ki}^t = \frac{\delta_{ki}^t}{\delta_{ki}^{t-1} - \delta_{ki}^t} \Delta w_{ki}^{t-1} \tag{5}$$

where Δw_{ki}^t and δ_{ki}^t is the weight correction and error at step t for neuron k of layer i.

Experimental sets are submitted to the neural network until a stabilization of the residual error is obtained at the output pattern. To this stabilization, a stopping criterion is applied concerning a fixed calculation duration, which is 1000 cycles. Neural number in both hidden layers is optimized consequently by comparing residual errors for each structure. For a given optimization, the number of experiments must be large enough to fix the weight values. Following the probably approximately correct (PAC) theory [13], this number must be ten times larger than weight values in the network structure:

$$N_{\mathrm{P}} = 10W \tag{6}$$

where N_{P} is the number of experiments and W is the number of weights in the network structure.

Instead of considering PAC theory which is quite restrictive, other authors suggested several expressions based on a correlation to input and output patterns [14]. This brings the number of experiments to rescannable value:

$$N_{\mathrm{H}} \in \left[\frac{N_{\mathrm{P}} N_{\mathrm{S}}}{N_{\mathrm{I}} + N_{\mathrm{S}}}, \frac{2N_{\mathrm{S}} N_{\mathrm{P}}}{N_{\mathrm{I}} + N_{\mathrm{S}}} \right] \tag{7}$$

where N_{H} is the number of neurons in the hidden layers. N_{P} is the number of cases submitted to the network. N_{I}

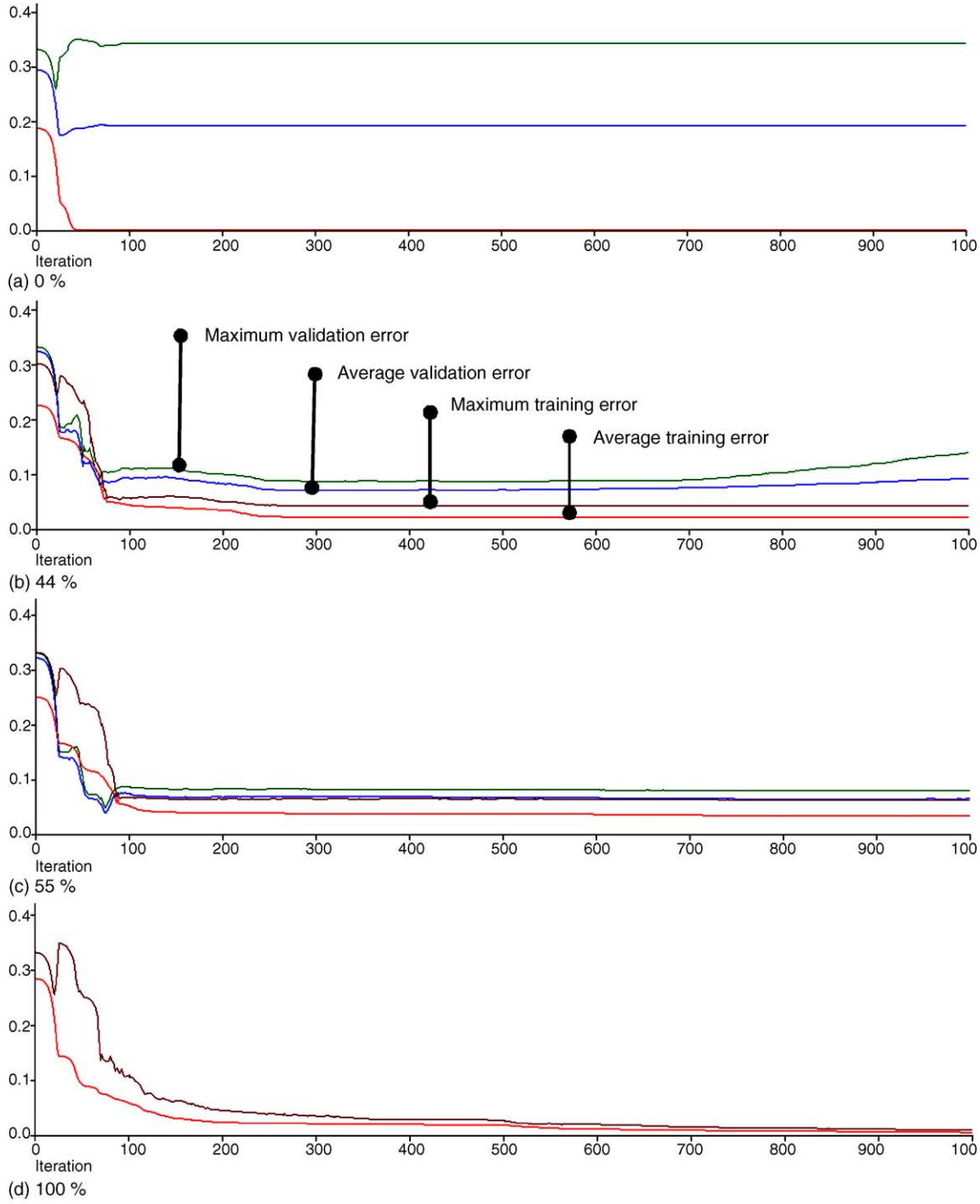

Fig. 1. Evolution of the optimization error as function of the size of the test sets.

and N_S are the number of neurons in the input and output layers.

Other studies permitted to estimate the number of experiments as falling within the range [11]:

$$W < N_P \leq 5W \tag{8}$$

In the case of this study, the number of experiments was nine (Table 2). The experimental sets were considered as original sets enlarged to take into account the standard deviation associated to input and output parameters [11]:

$$(O_j, I_j)_{new} = (O_k, I_k)_{original} \pm \text{ALEA}()(\sigma(o_k), \sigma(i_k)) \tag{9}$$

where O and I are related to neurons in the input and output layers, j and k are the indexes of samples in the new and original databases, respectively, ALEA() is a random number generator producing a Gaussian distribution around 0, and σ is the standard deviation associated to input and output units.

Table 2
Experimental and predicted results of crystallite size, coercivity and percentage of the cubic phase as function of milling conditions for nanocrystalline Co material

ω (rpm)	Ω (rpm)	Experimental predicted relative scatter (%)		
		D (μm)	C (%)	Hc
50	150	111	0	135
		112	1	134
		1.3	–	0.8
200	150	136	0	137
		135	2	138
		1.0	–	0.8
400	150	203	45	196
		203	45	196
		0.2	0.1	0.1
50	250	86	8	51
		83	7	53
		3.2	13.2	3.8
200	250	74	11	37
		77	10	37
		4.6	7.5	0.4
400	250	76	11	32
		76	12	31
		0.1	4.9	3.5
50	350	82	8	50
		81	9	48
		1.1	9.3	4.2
200	350	76	12	29
		75	12	34
		0.7	2.9	15.7
400	350	73	14	29
		73	14	27
		0.2	2.3	5.7

The ratio of enlargement depends on the variability of the process and varies generally between 5 and 20. In this study, this ratio was fixed to 15, permitting to obtain 135 new samples.

The validation of the ANN optimisation is included as test sets which are submitted during the training process. These are a part of the optimisation but weight parameters are not corrected when submitting a test set. In such a way, several runs were performed by varying the number of samples in the test procedure. Fig. 1 illustrates the evolution of the optimisation error (i.e., residual error), which is a combination of test and training errors, as function of the simulation time.

When there is no test sample in the database, the optimisation error was found to be the highest. This is particularly due to the lack of information as can be seen from Fig. 1a. When increasing the number of test samples, the optimisation error decreases and stabilise for a test database representing a ratio of 55% from the whole database (Fig. 1c). Finally, when the whole database was dedicated to training procedure (Fig. 1d), the optimisation error is the lowest possible but the validation of the results is rendered difficult as no sample test was included. This risk of learning case by case is eliminated by considering the optimised ANN structure considering a minimal test database representing 55% of the total samples.

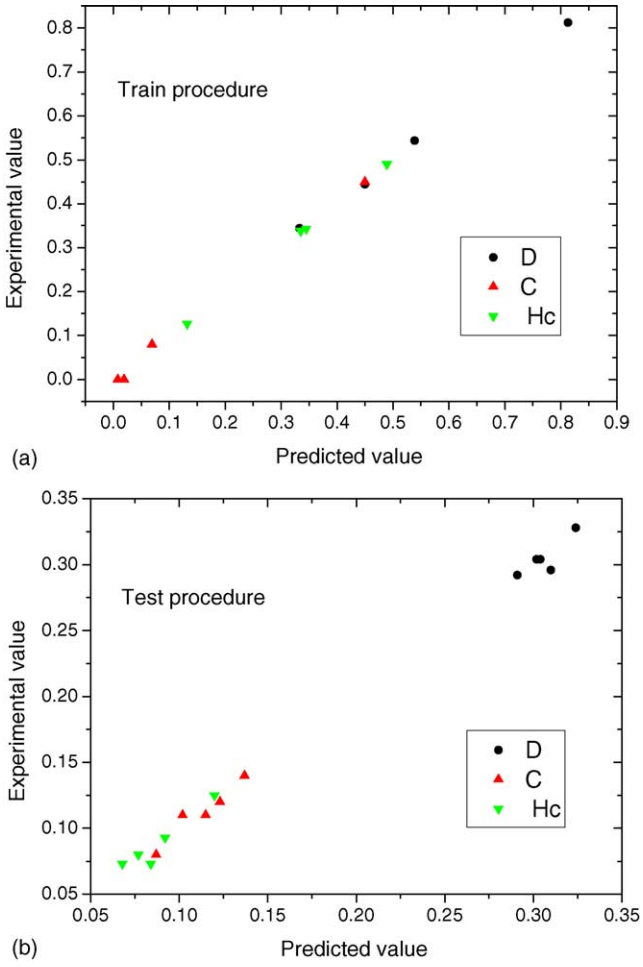

Fig. 2. Linearity between predicted and experimental results in the case (a) training and (b) test procedures. Test samples represents 55% from the whole database.

This compromise was found to be quite satisfactory as the test and training results were found to converge. Linearity between experimental and predicted responses was established as shown in Fig. 2.

4. Results and discussion

The optimization process of the neural network permitted to obtain a configuration with three neurons in the first hidden layer and four neurons in the second hidden layer (Fig. 3). The residual error was 0.007 and 100% of the submitted cases were learnt correctly (output errors were less than 5%). Table 2 compares the predicted and experimental results for crystalline size, percentage of cubic phase and coercivity. Average errors are 1, 6 and 4% for the studied parameters, respectively. The highest scatter for these does not exceed 16%.

By varying input values of the optimized ANN structure, it is possible to establish the combined effect of Ω and ω on crystallite size, cubic phase ratio and coercivity. Figs. 4–6

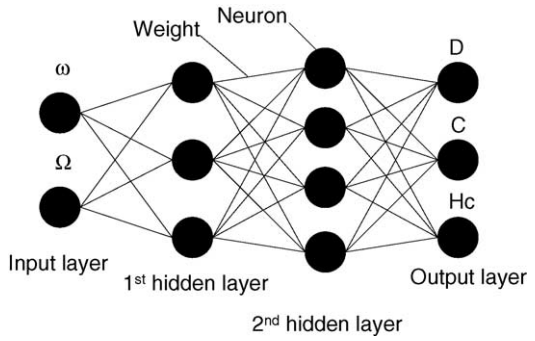

Fig. 3. The optimized ANN structure considered in this study.

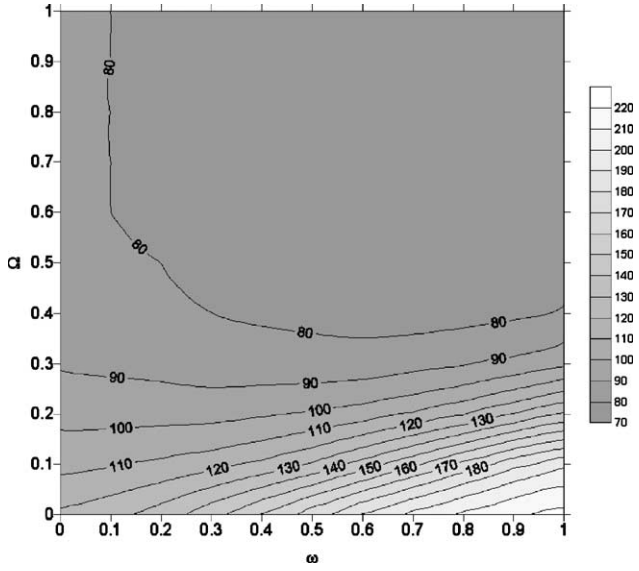

Fig. 4. Predicted counterplot of crystalline size as function of the milling conditions (Ω, ω).

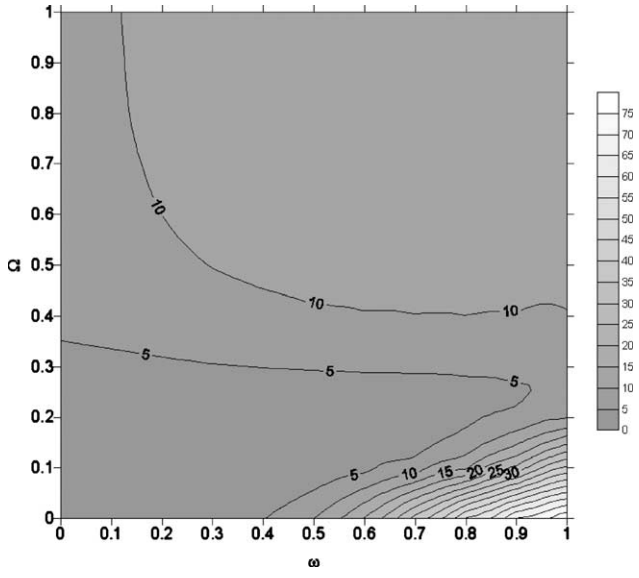

Fig. 5. Predicted counterplot of cubic phase percentage as function of the milling conditions (Ω, ω).

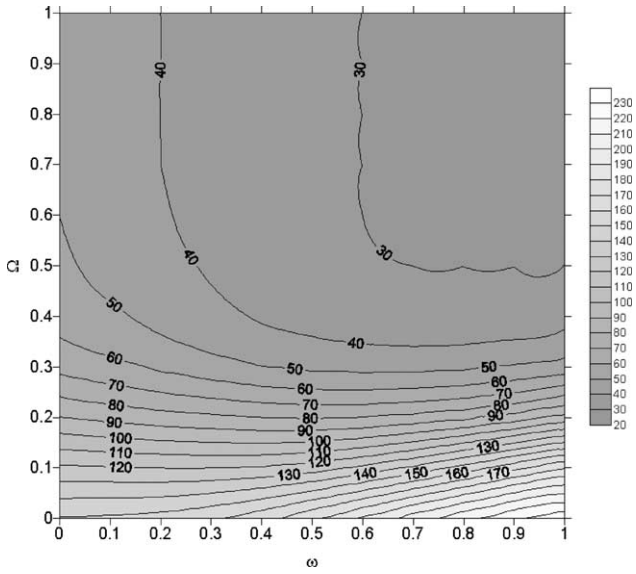

Fig. 6. Predicted counterplot of coercivity as function of the milling conditions (Ω, ω).

present, in a reduced form, the counterplots of the ANN responses in the defined parameter domains (Table 1). It is noticed that ANN response is more sensitive to ω variation especially in the case of crystallite size and coercivity. Values of plateau velocity greater than 0.4 (203 rpm) do not permit to obtain significant effect. This result is validated by comparing the predicted results with those of Huang et al. [8] for $\Omega = 160$ rpm (Table 3). Roughly speaking, the result of Huang et al. [8] put in evidence the formation of fcc phase without quantifying accurately the percentage of the phase. With the predicted results, it was possible to establish the variation of the cubic phase with a large variation for $\omega >$ 360 rpm.

Fig. 5 shows that only a small range of Ω and ω permit to increase the cubic phase proportion. The initial phase proportion was about 50%, as determined by XRD analysis [10]. The formation of fcc Co was first attributed to the Fe contamination arising from the steel balls and vials used during the milling [15]. However, this possibility was ruled out when the processing was carried out in agate vials and balls and hcp Co was still partially converted to fcc Co [10]. Recently, Sort et al. [16] showed that the stacking fault formation, rather than the local temperature rise, the impurity contamination or crystallite size reduction associated with the milling process, is the main mechanism governing the hcp–fcc transformation [16].

Table 3
The role ω of on the formation of the cubic phase

	ω (rpm)			
	124	243	361	440
Experimental [8]	hcp	hcp	hcp > fcc	fcc > hcp
Predicted percentage of hcp phase (%)	99	98	86	58

Comparison between experimental and predicted results for $\Omega = 160$ rpm.

One can conclude that the most significant changes on cubic phase ratio, crystallite size and consequently coercivity were obtained for $\omega/\Omega \gg 1$.

5. Summary

The effect of ball milling parameters on the microstructure of Co and consequently on the magnetic properties has been studied. The optimization process of the neural network has shown a good correlation with the experimental results. The combination of low values of Ω and high vial velocities ω can enhance the cubic phase formation. Predicted results showed that the most significant changes in the cubic phase ratio, crystallite size and coercivity were observed for $\omega/\Omega \gg 1$.

References

[1] B.S. Murty, S. Ranganathan, Int. Mater. Rev. 43 (1998) 101.
[2] A.R. Troiano, J.L. Tokich, Trans. Am. Inst. Miner. Metall. Petrol. Eng. 175 (1948) 728.
[3] C.R. Houska, B.L. Averbach, M. Cohen, Acta Metall. 33 (1985) 1293.
[4] P. Tolédano, G. Krexner, M. Prem, H.P. Weber, V.P. Dmitriev, Phys. Rev. B 64 (2001) 144104.
[5] E.A. Owen, DM. Jones, Proc. Phys. Soc. B 67 (1954) 456.
[6] C.G. Granqvist, R.A. Buhrman, J. Appl. Phys. 47 (1976) 2200.
[7] O. Kitakami, T. Sakurai, Y. Miyashita, Y. Takeno, Y. Shimada, H. Takano, et al., Jpn. J. Appl. Phys. 35 (1996) 1724.
[8] J.Y. Huang, Y.K. Wu, H.Q. Ye, Appl. Phys. Lett. 66 (1995) 308.
[9] J. Sort, S. Surinach, J.S. Munoz, M.D. Baro, M. Wojcik, E. Jedryka, S. Nadolski, N. Sheludko, J. Nogues, Phys. Rev. B 68 (2003) 014421.
[10] N.E. Fenineche, O. El Kedim, E. Gaffet, J. Metast. Nanocryst. Mater. 2000 (2000) 41–48.
[11] S. Guessasma, G. Montavon, C. Coddet, Comput. Mater. Sci. 29 (2004) 315–333.
[12] D. Patterson, Artificial Neural Networks, Prentice-Hall, Singapore, 1996.
[13] L. Valiant, Commun. ACM 27 (12) (1984) 1134.
[14] G. Brightwell, C. Kenyon, H. Paugam-Moisy, NeuroCOLT Technical Report Series, NC-TR-97-001, ESPRIT Working Group in Neural and Computational Learning, Dep. Comput. Sci., University of London, 1997.
[15] F. Cardellini, G. Mazzone, Phil. Mag. A67 (1993) 1289–1300.
[16] J. Sort, J. Nogues, S. Surinach, M.D. Baro, Phil. Mag. 83 (4) (2003) 439–455.